Magnetic bistability and Overhauser shift of conduction electrons in gallium oxide

Eric Aubay and Didier Gourier*
Laboratoire de Chimie Appliquée de l'Etat Solide, Ecole Nationale Supérieure de Chimie de Paris, 11, rue Pierre et Marie Curie, 75231 Paris CEDEX 05, France
(Received 8 December 1992)

We study the intrinsic magnetic bistability of conduction-electron spins in gallium oxide β-Ga_2O_3 by electron-paramagnetic-resonance (EPR) spectroscopy. This compound, normally an insulator, becomes an n-type semiconductor when synthesized under reducing conditions. The crystals studied in this work have a conductivity of 180–200 $\Omega^{-1}\,cm^{-1}$ at room temperature and 140 $\Omega^{-1}\,cm^{-1}$ at liquid-helium temperature. It has been previously shown [J. Phys. Chem. **96**, 5513 (1992)] that the hyperfine interaction between conduction-electron spins and nuclear spins of gallium is responsible for a strong dynamic nuclear polarization when the EPR of conduction electrons is saturated (Overhauser effect). The resulting nuclear field acting on the electron spins was found to be bistable, which causes a hysteresis of the resonance line. In this work we demonstrate that hysteresis can be theoretically produced by three different control parameters: the external magnetic field B_0, the microwave frequency ν, and the microwave field B_1 (or the microwave power P). A model is presented for the EPR line shape under bistable dynamic nuclear polarization, which is in fair agreement with experimental results for gallium oxide. We verify in this compound the existence of hysteresis of the EPR intensity upon positive and negative variations of the incident microwave power. The effect of sample size on bistability is also investigated. It is shown that this phenomenon can disappear if the sample size is larger than the skin depth of the compound. Bistability at room temperature in gallium oxide is found to be very sensitive to this size effect. The Overhauser shift of conduction electrons is also studied as a function of temperature. This parameter gives details on the hyperfine interaction between charge carriers and magnetic nuclei despite the extreme motional narrowing of the EPR line. The results are interpreted in terms of electronic transport at low temperatures involving an impurity band formed by oxygen vacancies acting as shallow donors.

I. INTRODUCTION

A conduction electron is the simplest microscopic object that can exhibit a bistability effect upon interaction with an electromagnetic field. Bistability means that for a given value of a control parameter, the system can occupy two possible steady states. An evident manifestation of bistability is the response of a system that is different for positive and negative variations of the control parameter. Such hysteresis is the main signature of a bistable system. Hysteresis due to single-electron bistability has been recently observed in the cyclotron resonance of InSb.[1] In this experiment, the cyclotron kinetic energy (the response) exhibits a hysteresis upon upward and downward sweeps of the driving frequency (the control parameter). This bistability originates from the relativistic mass increase of the electron. Another kind of conduction-electron bistability, observable by electron-paramagnetic resonance (EPR), has been briefly discussed by Kaplan[2] and qualitatively observed by Gueron and Ryter[3] in metallic lithium microparticles at the end of the 1950s. In that case, the response is the microwave power absorbed by electron spins and the control parameter is the external magnetic field B_0. This effect was however largely ignored during the following three decades. Recently, we demonstrated that the spin resonance of conduction electrons in semiconducting crystals of gallium oxide β-Ga_2O_3 exhibits hysteresis observable even at room temperature.[4]

The physical principle governing this electron-spin bistability can be described as follows. Let us first consider a free electron with spin $S=1/2$ in the conduction band of a solid. If it is submitted to an external magnetic field B_0, the effective spin Hamiltonian of the electron in the field is $H=g\beta B_0 S_z$ where g is the electron g factor, β is the electronic Bohr magneton, and S_z is the component of the electron spin along B_0. The eigenvalues of H give the two energy levels $E_\pm=\pm(1/2)g\beta B_0$ of the electron, where $m_s=\pm 1/2$ are the two possible values of S_z. If the electron is also submitted to a microwave magnetic field B_1, a transition between the two m_s states occurs if the resonant condition $h\nu=g\beta B_0$ is satisfied. With this simple system, the resonance condition does not depend on the sweeping direction of B_0 [Fig. 1(a)]. In that case, the conduction electron submitted to fields B_0 and B_1 is monostable since the resonance exhibits no hysteresis. If the solid also contains nonzero nuclear spins I, each nucleus can interact with S by the hyperfine interaction A, which is close to zero because of the strong electron delocalization. However, a single conduction electron interacts with a large number of nuclei N, which finally results in a small polarization of the nuclear spins. The partially polarized nuclei create a magnetic nuclear field B_n, which adds to the external field B_0. It is negligible at room temperature, and becomes significant only at very low temperatures. This nuclear polarization can be considerably enhanced by the Overhauser effect,[2,3,5] which occurs if the transition between the m_s electron states is partially saturated. With the Overhauser effect, the electron spins are thus submitted to an effective field

$B_{\text{eff}}=B_0+B_n$, which can be significantly different from B_0 for strong nuclear polarization, so that the electron-spin energy levels are now given by $E_{\pm}=\pm\frac{1}{2}g\beta B_{\text{eff}}$. The nuclear field B_n satisfies an equation of the type $B_n=f(B_n,B_0,B_1,\nu)$, which can have one or three solutions[2,4] for given values of B_0, B_1, and ν. The system is monostable if there is only one steady-state value of B_n. In that case the resonance condition $h\nu=g\beta(B_0+B_n)$ is still satisfied with upward and downward variations of B_0, and no hysteresis occurs. The evident manifestation of dynamic nuclear polarization is that the EPR line is shifted by an amount equal to the nuclear field. This is the Overhauser shift.[3,5] With this effect, the electron-spin energy levels are no longer linear in B_0, since B_n is a function of itself and of B_0 and ν. A schematic energy-level diagram (not to scale) corresponding to this situation is shown in Fig. 1(b). If equation $B_n=f(B_n,B_0,B_1,\nu)$ has three solutions, the spin system is bistable because one steady state of the nuclear field is unstable. This situation arises if the hyperfine interaction

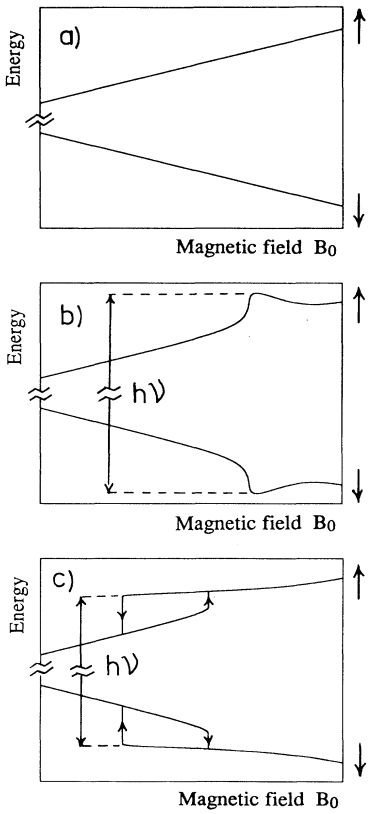

FIG. 1. Schematic energy-level diagrams (not to scale) for an electron spin $S=1/2$ in a magnetic field B_0. The energies are $E_{\pm}=\pm(\frac{1}{2})g\beta B_{\text{eff}}$, where B_{eff} is the effective magnetic field seen by the electron spin. (a) Free-electron spin: $B_{\text{eff}}=B_0$. (b) and (c) free-electron spin under Overhauser effect, submitted to a microwave field B_1 of frequency ν: $B_{\text{eff}}=B_0+B_n$, where $B_n=f(B_n,B_0,B_1,\nu)$ is the nuclear field. (b) and (c) correspond, respectively, to monostable and bistable nuclear fields. In both cases, the nonlinear features are intentionally exaggerated. The two spin states are marked by arrows.

is strong enough, and if the transverse electron relaxation time T_2 is sufficiently long.[7] The resulting variation of B_n with B_0 exhibits an S-shaped curve typical of bistable systems.[4] This bistable regime implies that the splitting $g\beta B_{\text{eff}}$ of the two electron-spin states submitted to B_0 and to the saturating microwave field B_1 exhibits discontinuous jumps at characteristic switching thresholds, which are different for positive and negative variations of B_0. This situation is schematized in Fig. 1(c). Note that the nonlinear features in Figs. 1(b) and 1(c) are overamplified for the sake of clarity, since generally $B_n \ll B_0$.

The occurrence of bistable electron-spin resonance has been observed in lithium microparticles[3] at 4 K and in gallium oxide at temperatures up to 300 K.[4] In the latter compound, conduction electrons originate from oxygen vacancies acting as shallow donors,[8] and the nuclear polarization concerns gallium nuclei ^{69}Ga (60.1%, $g_n=1.34439$) and ^{71}Ga (39.9%, $g_n=1.70818$) with spins $I=3/2$. However, several points that have not been addressed in Ref. 4 are the object of this paper:

(i) In addition to B_0, the microwave frequency ν and the microwave field B_1 (or the incident microwave power P) can in principle be used as control parameters of the bistable spin system. We demonstrate that they can actually be responsible for hysteresis of the EPR signal.

(ii) The EPR lines in a bistable regime are very distorted and exhibit unusual shapes. A full understanding of the bistability itself can only be achieved by accurate simulation of these lines.

(iii) It is not clear why gallium oxide possesses electron-spin bistability up to room temperature, which to the best of our knowledge is without precedent. Since this property is limited to conduction electrons, the explanation should be found in some distinctive characteristics of the electronic structure of this compound. The Overhauser shift is suitable to measure hyperfine interaction between conduction-electron spins and lattice nuclei, where EPR lines show neither hyperfine interaction nor inhomogeneous broadening. Since the hyperfine interaction is very sensitive to the nature of the electronic wave function, the Overhauser shift in gallium oxide should provide information about its electronic structure in relation to its transport properties.

In what follows we extend in Sec. II the theory of the electron-spin bistability to the three control parameters B_0, ν, and P. The sample preparation, in relation with the origin of defects is described in Sec. III. Section IV A deals with the study of the temperature dependence of the relaxation times T_1 and T_2, and of the hyperfine interaction. Hysteresis induced by magnetic-field sweeping is investigated in details in Sec. IV B, where simulations of bistable EPR lines are given. Section IV C deals briefly with the effect of sample size on bistability. In Sec. IV D, we demonstrate that the EPR intensity exhibits a strong hysteresis upon variation of the incident microwave power, as predicted in Sec. II.

II. CONDUCTION-ELECTRON-SPIN BISTABILITY

We present in this section the principle of conduction-electron-spin bistability. We show that in addition to the

external magnetic field B_0, other parameters such as microwave frequency ν and microwave power P can be used as control parameters to produce a bistable hysteresis of the electron-spin resonance.

To start with, let us consider a conduction-electron spin $S=1/2$ interacting with N equivalent lattice nuclear spins I via the scalar hyperfine interaction A. The ensemble average of the nuclear spins over the N nuclei is the nuclear polarization $\langle I_z \rangle$, given by

$$\langle I_z \rangle = \frac{1}{N} \sum_{k=1}^{N} \langle I_{z,k} \rangle , \tag{1}$$

where $\langle I_{z,k} \rangle$ is the time average of the polarization of the kth nucleus. The nuclear polarization induces a nuclear field B_n acting on the electron spin, in addition to the external field B_0:

$$B_n = \frac{NA}{g\beta} \langle I_z \rangle . \tag{2}$$

The steady-state mean value of the electron spin $\langle S_z \rangle$ is related to the electronic saturation factor s by the following expression:

$$s = \frac{\langle S_z^0 \rangle - \langle S_z \rangle}{\langle S_z^0 \rangle} , \tag{3}$$

where $\langle S_z^0 \rangle$ is the thermal equilibrium value of $\langle S_z \rangle$. The saturation factor can vary between 0 for thermal equilibrium and 1 for complete saturation. The electron-spin polarization $\langle S_z \rangle$ can be deduced from the Bloch equations,[9] which lead to the following general expression for the saturation factor:[2,4]

$$s = \frac{\gamma^2 T_1 T_2 B_1^2}{1+\gamma^2 T_1 T_2 B_1^2 + \gamma^2 T_2^2 (B_{\text{eff}} - h\nu/g\beta)^2} , \tag{4}$$

in which we replaced B_0 by $B_{\text{eff}} = B_0 + B_n$, the effective magnetic field acting on the electron spin. $\gamma = g\beta/\hbar$ is the electronic gyromagnetic ratio. The microwave field B_1 is related to the incident microwave power P by $P = KB_1^2$, where K is a constant dependent upon the EPR cavity. At low microwave power, both electronic and nuclear polarizations are close to thermal equilibrium. In the high-temperature limit, $\langle S_z \rangle$ and $\langle I_z \rangle$ are given by

$$\begin{aligned} \langle S_z \rangle &\approx \langle S_z^0 \rangle = -\frac{g\beta B_0}{4kT} , \\ \langle I_z \rangle &\approx \langle I_z^0 \rangle = \frac{g_n \beta_n I(I+1) B_0}{3kT} , \end{aligned} \tag{5}$$

where g_n is the g factor of the nucleus of spin I. At high temperature, the very small nuclear polarization results in a negligible nuclear field. For example, B_n is smaller than 10^{-3} mT between 100 K and room temperature in β-Ga_2O_3 at thermal equilibrium.[4] The nuclear polarization can be considerably enhanced by dynamic nuclear polarization (DNP) via saturation of the EPR line (Overhauser effect).[5] If the $\Delta m_s = \pm 1$ EPR transition is partially saturated at strong microwave power, $\langle S_z \rangle$ decreases from its equilibrium value. If, on the other hand, the nuclear relaxation occurs mainly by a flip-flop mechanism $\Delta(m_s + m_I) = 0$ with a characteristic time T_x, the change of electron-spin polarization is transferred to nuclear spins, giving the following nonequilibrium nuclear polarization:[5,6]

$$\langle I_z \rangle = (\langle S_z \rangle - \langle S_z^0 \rangle) \frac{I(I+1)}{S(S+1)} f ,$$

with

$$f = \frac{1/T_x}{1/T_x + 1/T_n} . \tag{6}$$

f is the leakage factor, which reflects the efficiency of the

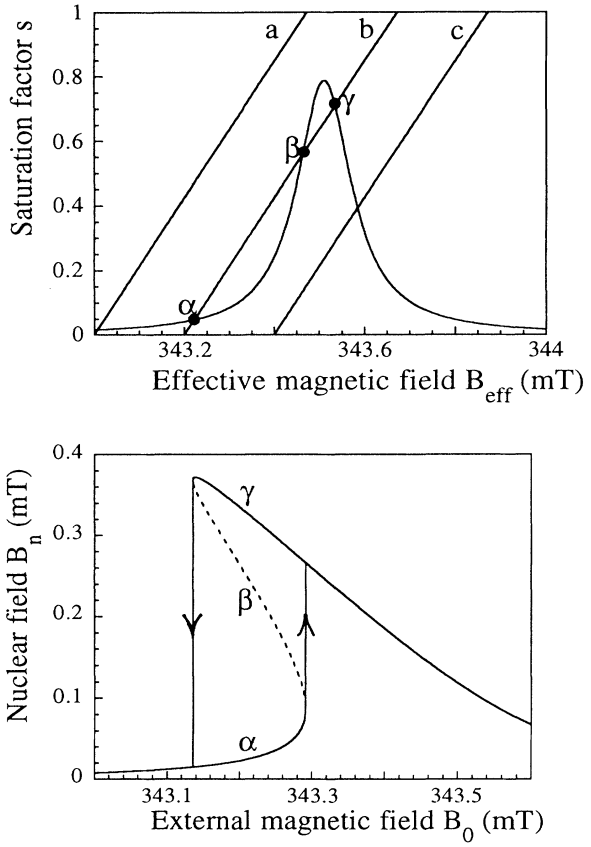

FIG. 2. Magnetic-field induced hysteresis. These figures represent the variation of the saturation factor s vs the effective magnetic field B_{eff} (top) and of the nuclear field B_n vs B_0 (bottom). The latter is obtained by numerical resolution of Eq. (12). The Lorentzian curve and the straight line represent expressions (4) and (10), respectively. Lines a, b, and c correspond to three selected values of the external magnetic field B_0, 343, 343.2, and 343.4 mT, respectively. (b) corresponds to a bistability situation. The other parameters are the electron-spin relaxation times $T_1 = T_2 = 2.0 \times 10^{-7}$ s, $(\Delta B_{\text{ov}})_{\text{max}} = 0.473$ mT, the microwave field $B_1 = 0.056$ mT, and the microwave frequency $\nu = 9437$ MHz. These parameters correspond to experimental values for β-Ga_2O_3 at 150 K. The possible values of B_{eff} are given by the crossing points of the straight line and the Lorentzian curve. Points α, β, and γ correspond to the three steady states of the spin system in bistable regime.

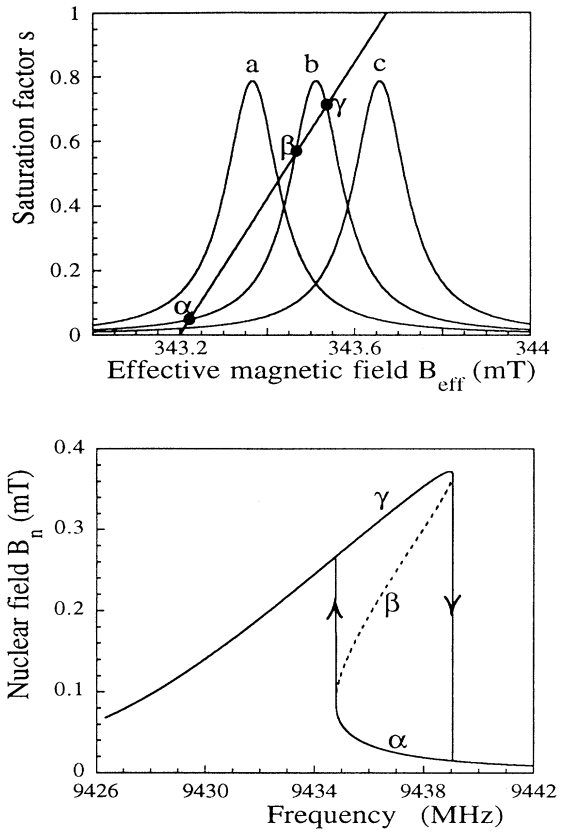

FIG. 3. Microwave frequency-induced hysteresis. These figures represent the variation of the saturation factor vs the effective magnetic field B_{eff} (top) and of the nuclear field B_n vs microwave frequency (bottom). The position of the straight line corresponds to $B_0=343.2$ mT. Curves *a*, *b*, and *c* correspond to microwave frequencies $\nu=9433$, 9437, and 9441 MHz, respectively. (b) corresponds to a bistability situation. Parameters T_1, T_2, B_1, and $(\Delta B_{\text{ov}})_{\text{max}}$ are identical to those of Fig. 2.

flip-flop relaxation mechanism. In expression (6), T_n represents all the other nuclear relaxation times. The optimal situation corresponds to $f=1$, which is favored when A is a purely Fermi-type interaction:

$$A=(8\pi/3)h^{-1}g\beta g_n\beta_n|\Psi_0|^2 , \tag{7}$$

where $|\Psi_0|^2$ is the electron-spin density at each of the N equivalent nuclei. Taking into account expression (6) for the nuclear polarization, the saturation factor s [expression (3)] becomes

$$s=-\frac{S(S+1)}{I(I+1)}\frac{\langle I_z\rangle}{\langle S_z^0\rangle}\frac{1}{f} . \tag{8}$$

From expressions (2) and (5) for $\langle I_z\rangle$ and $\langle S_z\rangle$, expression (8) becomes

$$s=\frac{3kT}{I(I+1)}\frac{B_{\text{eff}}-B_0}{NAfB_0} , \tag{9}$$

which can be simplified to

$$s=\frac{B_{\text{eff}}-B_0}{(\Delta B_{\text{ov}})_{\text{max}}} , \tag{10}$$

with

$$(\Delta B_{\text{ov}})_{\text{max}}=\frac{I(I+1)NAfB_0}{3kT} . \tag{11}$$

The parameter $(\Delta B_{\text{ov}})_{\text{max}}$ corresponds to the largest theoretical value of the nuclear field, which is obtained for complete saturation. Expressions (4) and (10) form a complete set of equations, the resolution of which gives the possible values of the effective magnetic field acting on electron spins. For constant values of all the parameters in these expressions, the steady-state solutions for B_{eff} can exhibit either a single value, and the spin system is monostable, or three values, which results in bistability (since one out of these three solutions is unstable). These equations can be resolved graphically. Expressions (4)

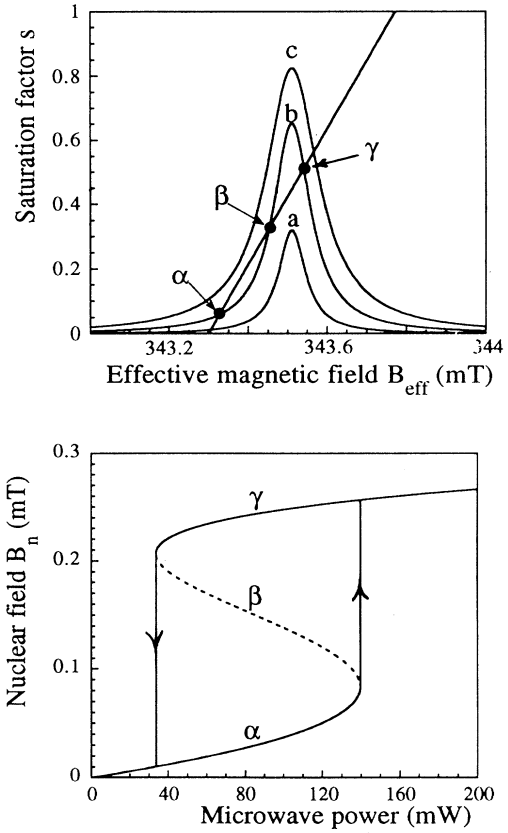

FIG. 4. Microwave field (or microwave power) induced hysteresis. These figures represent the variation of the saturation factor vs the effective magnetic field B_{eff}(top) and of the nuclear field B_n vs incident microwave power P (bottom). The position of the straight line corresponds to $B_0=343.3$ mT. Curves *a*, *b*, and *c* correspond to microwave field values $B_1=0.020$, 0.039, and 0.062 mT, respectively. (b) corresponds to a bistability situation. The field B_1 is related to P by the relation $P=5.2\times10^4 B_1^2$. Parameters T_1, T_2, ν, and $(\Delta B_{\text{ov}})_{\text{max}}$ are identical to those of Fig. 2.

and (10) are controlled by eight parameters which can be separated into two classes: those inherent to the structure and properties of the solid and those which can be controlled experimentally. The material-dependent parameters are the electronic relaxation times T_1 and T_2, the leakage factor f, which depends on the nuclear relaxation times, the electron g factor, and the parameter $(\Delta B_{ov})_{max}$. The influence of these parameters on bistability has been dealt with in another paper.[7] The experimental control parameters are B_0, the microwave power P (or the microwave field B_1), the microwave frequency ν, and the temperature T. We show now that B_0, P, and ν can produce a hysteresis effect on the EPR. Temperature is also a possible control parameter which in principle can produce a hysteresis of the nuclear field. However, the phenomenon becomes more complicated because the variation of temperature results in a variation of electronic and nuclear relaxation times in addition to a variation of the thermal nuclear polarization.

Figures 2–4 show the graphical solutions of Eqs. (4) and (10), which are represented by the Lorentzian curve and the straight line, respectively. Note, however, that expression (10) for $s=f(B_{eff})$ is not linear, since $(\Delta B_{ov})_{max}$ is a function of $B_0=B_{eff}-B_n$. However, if we consider the range of the magnetic field B_0 corresponding to the resonance of conduction electrons in β-Ga_2O_3, typically 1 mT, the deviation from linearity given by $\Delta B_{eff}/B_{eff}$ does not exceed 0.3%. If the straight line crosses the Lorentzian at a single point, only one solution for B_{eff} results, and the system is monostable. On the other hand, in the case of three crossing points, the spin system has three steady states α, β, and γ, which correspond to a situation of bistability (the β state being unstable). Figures 2–4 also show the resulting variations of B_n as a function of B_0, ν, and P, respectively. The exact expression for B_n is obtained from expressions (4) and (10):

$$B_n=(\Delta B_{ov})_{max}\frac{\gamma^2T_1T_2B_1^2}{1+\gamma^2T_2^2(B_n+B_0-h\nu/g\beta)^2+\gamma^2T_1T_2B_1^2}\ . \tag{12}$$

This equation was numerically solved with values of T_1, T_2, and $(\Delta B_{ov})_{max}$ corresponding to the particular case of β-Ga_2O_3 at 150 K (see Sec. IV A).

Let us now consider successively the three possible cases of hysteresis.

(i) Hysteresis induced by magnetic-field sweep (Fig. 2). This situation has been considered in our previous paper,[4] and is recalled here only for the sake of clarity. The variation of B_0 corresponds to a horizontal translation of the straight line [expression (10)] while the Lorentzian curve [expression (4)] has fixed position and amplitude, corresponding to constant values of ν and P. The resulting variation of B_n with B_0 has the form of an S-shaped curve bent toward low field, with a middle branch corresponding to the unstable state β. Sweeping up or down the magnetic field results in abrupt transitions from the α to the γ state and from the γ to the α state, respectively, at different critical values of B_0 and without reaching the β state. These transitions result in jumplike changes of the electron-spin polarization $\langle S_z\rangle$, which are responsible for the hysteresis of the EPR.

(ii) Hysteresis induced by frequency sweep (Fig. 3). This case is symmetrical with the preceding one. The position of the straight line and the amplitude of the Lorentzian curve are kept constant, which corresponds to fixed values of B_0 and P, respectively. The variation of ν corresponds to a horizontal translation of the Lorentzian curve. Depending on the value of ν, one obtains one or three crossing points with the straight line. The resulting variation of B_n with ν also exhibits an S-shaped curve, bent toward high frequency. Sweeping upward and downward the microwave frequency should thus result in abrupt transitions between α and γ states, with hysteresis. However, we did not study experimentally this frequency sweep hysteresis because standard EPR spectrometers work at fixed frequency.

(iii) Hysteresis induced by variation of the incident microwave power (Fig. 4). The positions of the straight line and the Lorentzian curve are fixed in this case, and correspond to constant values of B_0 and ν. Increasing P corresponds to a broadening and an increase of the Lorentzian curve. One or three solutions are also obtained depending on the P value. Using the same parameters [T_1, T_2, and $(\Delta B_{ov})_{max}$] as for Figs. 2 and 3 leads to an S-shaped curve for $B_n=f(P)$. In a bistable regime, one thus expects jumplike variations of $\langle S_z\rangle$ at critical values of the microwave power, with a broad hysteresis. This phenomenon is demonstrated in Sec. IV D.

III. EXPERIMENTAL PART

Single crystals of β-Ga_2O_3 were obtained by the flame fusion process (Verneuil method), in which a single-crystal seed is fed by a powder passing through the flame of an oxhydric torch. The starting material was gallium oxide powder (purity 4N) from Rhone-Poulenc. This compound has an optical band gap of 4.84 eV and is thus normally an insulator[8] ($\sigma\approx10^{-6}\ \Omega^{-1}\,cm^{-1}$) and transparent. It becomes an n-type semiconductor when it is synthesized under reducing conditions. We used a H_2/O_2 flow of 2:3 in the Verneuil torch, giving a strongly reducing flame. During synthesis, a while smoke emanating from the crystal was due to the evaporation of Ga_2O according to the following reaction:[10]

$$(Ga_2O_3)_{solid}\rightarrow(Ga_{2-x}O_{3-y})_{solid}+\frac{x}{2}(Ga_2O)+\left[\frac{y}{2}-\frac{x}{4}\right]O_2\ , \tag{13}$$

with $y > x$. This reaction can be decomposed into two simple elementary ones involving point defects. The first one corresponds to the formation of oxygen vacancies compensated by two electrons, noted $V_O^{\times}$ centers in the Kröger-Vink notation or F centers in spectroscopic notation:

$$2O_O^{\times} \rightarrow 2V_O^{\times} + O_2 \ . \tag{14}$$

The second reaction corresponds to the production of the suboxide Ga_2O:

$$2Ga_{Ga}^{\times} + O_O^{\times} \rightarrow 2V_{Ga}^{\times} + V_O^{\times} + Ga_2O \ . \tag{15}$$

The oxygen vacancies form shallow donors[8] (donor ionization energy $E_d = 0.03-0.04$ eV) responsible for the n-type semiconductivity. Under these reducing conditions we obtained rod-shaped samples of about 1–7 cm length and 0.5–1 cm diameter, built of several monocrystalline platelets. These single crystals are transparent, slightly blue, and without apparent macroscopic defects. Because of their high conductivity, about 180–200 $\Omega^{-1}\,cm^{-1}$ at room temperature, we used only very small crystals (for example, $0.08 \times 1.8 \times 0.3$ mm^3) in order to avoid distortion of the EPR line by the skin-depth effect.[11]

The EPR spectra were recorded on a Bruker 220D spectrometer operating at X-band and equipped with the variable temperature accessory (100–300 K) and with an Oxford Instrument ESR 9 continuous flow cryostat (4–100 K). The concentration of unpaired conduction electron spins $N_s \approx 10^{19}$ cm^{-3} of our samples was determined by comparison with a standard diphenylpicrylhydrazyl (DPPH) sample fixed on the sample tube, and by using the following formula:

$$N_s = \frac{I_s}{I_{\text{ref}}} \frac{n_{\text{ref}}}{m} \rho \ , \tag{16}$$

where I_s and I_{ref} are the double integrals of the EPR lines of the sample and the reference, respectively, $\rho = 5.88$ $g\,cm^{-3}$ is the density of gallium oxide, m is the sample weight, and $n_{\text{ref}} = 1.5 \times 10^{17}$ spins is the number of spins in the DPPH sample.

The cavity constant K, defined as $P = KB_1^2$, was determined using a DPPH reference sample by the method described by Poole.[12] $K = 6.1 \times 10^4$ mW mT^{-2} and $K = 5.2 \times 10^4$ mW mT^{-2} were obtained for the cavity equipped with helium and nitrogen inserts, respectively.

IV. RESULTS AND DISCUSSION

A. Overhauser shift

At very low microwave power (for example, $P = 0.2$ mW, corresponding to a microwave field $B_1 = 2 \times 10^{-3}$ mT), the EPR spectrum at room temperature of a β-Ga_2O_3 single crystal consists of a single and very narrow Lorentzian line about 0.04 mT wide. The principal values of the g tensor are $g_z = 1.9635$, $g_x = 1.9590$, and $g_y = 1.9616$ with the z axis parallel to the crystallographic b axis. The x and y axes lie in the ac plane, the y and a axes making an angle of 30°. The components of the g tensor are independent of temperature from 4 to 300 K. In the following, all the reported phenomena correspond to the magnetic field B_0 oriented parallel to the b axis, except for the inset of Fig. 13. Upon increasing the microwave power P, the EPR line distorts and shifts to a low magnetic field as a result of the increase of the nuclear field created by the dynamic nuclear polarization. The effect is more important at low temperature. Figure 5 shows two series of spectra recorded with negative variations of B_0 for a range of microwave powers, at room temperature and at 150 K. With positive variation of B_0, the spectra are identical with those of Fig. 5 at low microwave power, but they exhibit different shapes and positions at high P because of the hysteresis due to the bistable nuclear field.

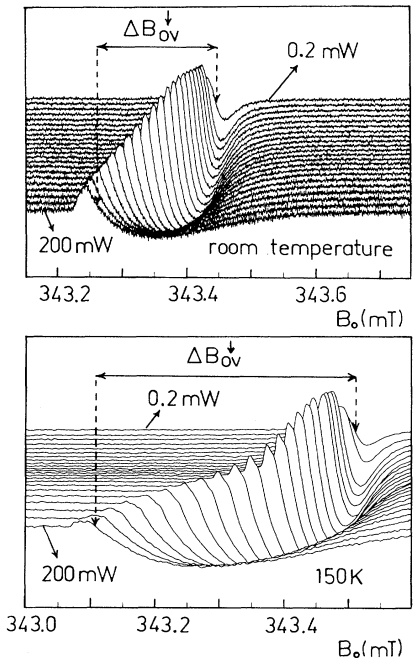

FIG. 5. Overhauser shift of the magnetic resonance of conduction electrons in β-Ga_2O_3 at room temperature (top) and at 150 K (bottom). All the spectra are recorded at decreasing variations of the external magnetic field B_0. For each stack plot, the spectra are recorded with the microwave attenuation increasing by steps of 1 dB from the bottom to the top of the figure and by steps of 5 dB for the two last ones. The microwave frequency is 9435.2 MHz at room temperature and 9437 MHz at 150 K. Sweeping time 100 s; time constant 41 ms; modulation amplitude 0.01 mT. $\Delta B_{\text{ov}}^{\downarrow}$ is the Overhauser shift under decreasing variation of B_0.

For a backward sweep at a given microwave power, the EPR intensity is zero at the center of resonance, which corresponds to the condition $B_n + B_0 = h\nu/g\beta$ in expression (12), as will be evident below [(expression (31)]. The shift of the center of the resonance upon increasing the microwave power, equal to the microwave field B_n, is called the Overhauser shift and noted $\Delta B_{\text{ov}}^{\downarrow}$:

$$\Delta B_{\text{ov}}^{\downarrow} = (\Delta B_{\text{ov}})_{\max} \frac{P}{a + P} \ , \tag{17}$$

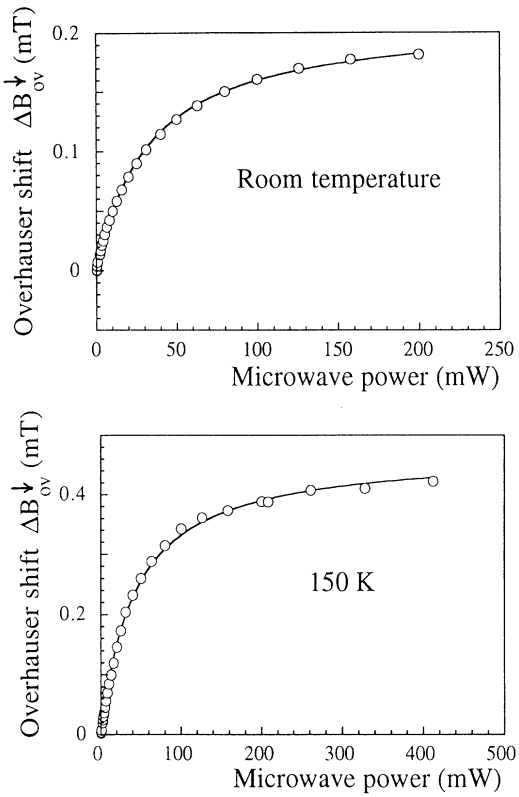

FIG. 6. Microwave power dependence of the Overhauser shift $\Delta B_{ov}^{\downarrow}$ measured under decreasing variation of B_0 at room temperature (top) and at 150 K (bottom). Open circles: experimental values. The solid lines correspond to the least-squares fits of the experimental points to expression (17). The adjustable parameters are $(\Delta B_{ov})_{max}$ and the constant a. Results at room temperature: $(\Delta B_{ov})_{max}=0.213\pm0.002$ mT and $a=33.3\pm0.7$ mW; correlation coefficient: 0.9995. Results at 150 K: $(\Delta B_{ov})_{max}=0.473\pm0.003$ mT and $a=43\pm1$ mW; correlation coefficient: 0.9994.

with

$$a=\frac{K}{\gamma^2 T_1 T_2} . \tag{18}$$

Expression (17) corresponds to the classical expression for the Overhauser shift,[3,13] however we have previously demonstrated that it is relevant only for a downward sweep of B_0 in bistable regime.[4] There is no equivalent simple analytical expression for the Overhauser shift $\Delta B_{ov}^{\updownarrow}$ recorded under the upward sweep of B_0. Figure 6 shows the microwave power dependence of $\Delta B_{ov}^{\downarrow}$ at room temperature and at 150 K. We recorded this type of variation for 27 different values of the temperature, ranging between 5 K and room temperature. For each temperature, the experimental variation $\Delta B_{ov}^{\downarrow}=f(P)$ was a least-squares fit to expression (17) with a and $(\Delta B_{ov})_{max}$ as adjustable parameters. The temperature dependence of T_2 was deduced from the peak-to-peak linewidth ΔB_{pp}^{0} of the unsaturated EPR line:

$$\Delta B_{pp}^{0}=\frac{2}{\sqrt{3}\gamma T_2} . \tag{19}$$

The temperature dependence of the spin-lattice relaxation time T_1 was obtained from expressions (18). The results are shown in Fig. 7. The first feature to note is that both T_1 and T_2 exhibit a very small temperature dependence. Moreover the equality $T_1\approx T_2$ is approximately satisfied between room temperature and about 100 K, and T_1/T_2 increases up to about 3 below 10 K. This indicates that the EPR is motionally narrowed even at liquid-helium temperature. This result agrees with conductivity measurements in our samples, showing that the value $\sigma\approx140\ \Omega^{-1}\,\mathrm{cm}^{-1}$ at 5 K is only slightly smaller than the room temperature value $\sigma\approx180$–$200\ \Omega^{-1}\,\mathrm{cm}^{-1}$. This conductivity, quasi-independent of temperature, is consistent with the observation of a bistable Overhauser shift in the temperature range 4–300 K.

The temperature dependence of $(\Delta B_{ov})_{max}$ is essentially dominated by its Curie-type behavior due to thermal polarization [expressions (11) and (5)], but it also contains the temperature dependence of parameters N, A, and f. According to expression (11), one can deduce from $(\Delta B_{ov})_{max}$ the product NAf, as shown in Fig. 8. This product varies only by a factor of 3 between 4–300 K. This observation is also consistent with the small difference between 4 K and room temperature conduc-

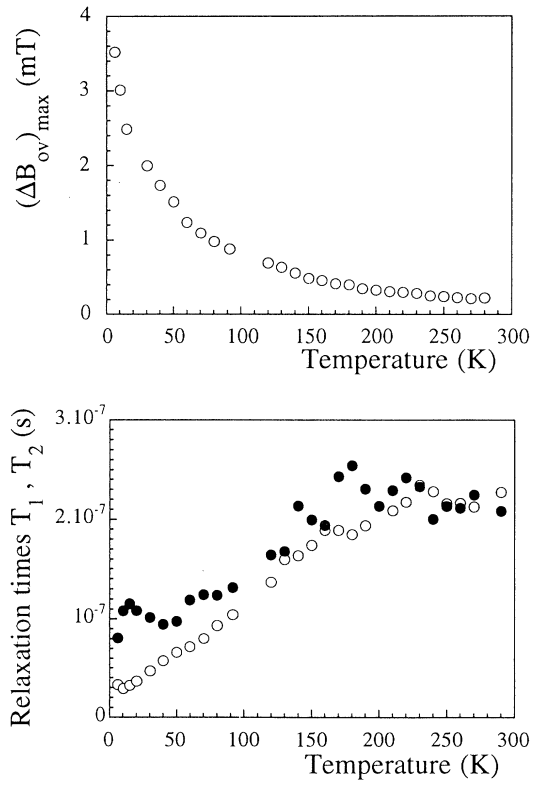

FIG. 7. Top: Temperature dependence of $(\Delta B_{ov})_{max}$. Bottom: temperature dependence of T_1 (black circles) and T_2 (open circles).

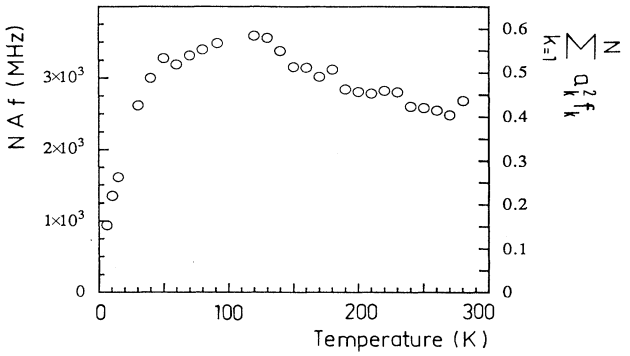

FIG. 8. Temperature dependence of the product NAf (left scale) obtained from Fig. 7 and expression (11) and of $\sum_{k=1}^{N} a_k^2 f_k$ obtained from expression (24) (right scale).

tivities in our samples. NAf first increases rapidly from 4 K to about 100–150 K, and next slowly decreases at higher temperature. There is no simple explanation for this variation since each of the three parameters N, A, and f can have its own temperature dependence. However, the presence of a maximum for NAf between 100–150 K indicates a change in the regime of electron transport at these temperatures, with σ decreasing with increasing T at high temperature. This "metallic" behavior is consistent with the observation of a quasiconstant value of T_1 and T_2 above 150 K (Fig. 7), and is confirmed by conductivity measurements performed on samples similar to ours[8] (containing about 2×10^{18} donors/cm^{-3}), and showing a decrease of σ above 120 K.

It should be noted that expression (11) is written for the simple case of an electron interacting with N equivalent nuclei, which considers neither the presence of two gallium isotopes, nor the existence of two different types of gallium sites (octahedral and tetrahedral) in the lattice[14] and also the possible nonuniform distribution of electron-spin density over each type of gallium site.

Let us write the electron state $|\phi\rangle$ in the conduction band as a linear combination of s,p, and d atomic orbitals of the N gallium atoms:[15]

$$|\phi\rangle=\sum_{k=1}^{N}[a_k|s_k\rangle+b_k|p_k\rangle+c_k|d_k\rangle], \tag{20}$$

where a_k, b_k, and c_k are the coefficients of the s_k, p_k, and d_k orbitals of the kth gallium atom. The main contribution to the scalar hyperfine interaction A_k with the kth nucleus is due essentially to the s_k orbital:

$$A_k=\frac{8\pi}{3}h^{-1}g\beta g_n\beta_n a_k^2|s_k(0)|^2=a_k^2A_0\ , \tag{21}$$

where $s_k(0)$ is the amplitude of the $4s$-wave function at the kth gallium nucleus. A_0 is the hyperfine interaction for a single Ga^{2+} ion [configuration $(4s)^1$]. If we take into account the two isotopes ^{69}Ga and ^{71}Ga, one must replace A_k by the average value $\langle A_k\rangle$:

$$\langle A_k\rangle=\sum_{i=1}^{2}p^{(i)}A_k^{(i)}=a_k^2\sum_{i=1}^{2}p^{(i)}A_0^{(i)}\ , \tag{22}$$

where the sum runs over the two isotopes. Taking into account these effects, expression (11) is still valid if we replace NAf by the average value $\langle NAf\rangle$:

$$\langle NAf\rangle=\sum_{k=1}^{N}\langle A_k\rangle f_k=\sum_{k=1}^{N}a_k^2f_k\sum_{i=1}^{2}p^{(i)}A_0^{(i)}\ . \tag{23}$$

Raüber[16] measured a hyperfine interaction $A\approx7800$ MHz for isolated $^{71}Ga^{2+}$ ions in ZnS. We may consider this value as a good estimation of A_0 for the $^{71}Ga^{2+}$ ion. Since the ratio of the interactions $A_0^{(i)}$ of the two isotopes is equal to the ratio of their g_n factor, expression (13) becomes

$$\langle NAf\rangle\approx6800\sum_{k=1}^{N}a_k^2f_k\ . \tag{24}$$

Finally, the temperature dependence of NAf is essentially determined by the sum $\sum a_k^2f_k$ where the three parameters N,a_k, and f_k can be temperature dependent. Figure 8 shows that the sum reaches its maximum value ≈0.6 at 100 K, and its minimum value ≈0.15 at liquid-helium temperature. If we note that its maximum possible value is 1, the results for gallium oxide show that the electron wave function is of predominantly $4s$ gallium character and that there is no significant leakage, which indicates that the nuclear relaxation is dominated by the mechanism $\Delta(m_s+m_I)=0$.

All these features can be rationalized if we assume that oxygen vacancies, which form shallow donors, are sufficiently concentrated to give rise to an impurity band. The latter is fully occupied if all the oxygen vacancies are neutral ($V_O^{\times}$ centers), as imposed by reactions (14) and (15). It can be partially occupied if acceptors are present in the compound. Vasil'tsiv[17] showed by fluorescence experiments the existence of such acceptors, which were attributed to vacancy pairs of the type $(V_O,V_{Ga})^{\times}$. These defects could result from an association of gallium and oxygen vacancies produced in reaction (15). They are however less abundant than free oxygen vacancies [$y>x$ in expression (13)]. A $V_O^{\times}$ center can transfer an electron to a $(V_O,V_{Ga})^{\times}$ defect according to the reaction

$$V_O^{\times}+(V_O,V_{Ga})^{\times}\rightarrow V_O^{\bullet}+(V_O,V_{Ga})'\ . \tag{25}$$

We thus propose that the overlap of $V_O^{\bullet}$ and $V_O^{\times}$ orbitals form a partially occupied impurity band. The relatively high conductivity at low temperature could thus involve only the electronic motion in this band. Upon increasing the temperature, electrons are progressively thermally excited in the conduction band, which results in the increase of T_1, T_2, and the product NAf. At high temperature, the carrier concentration in the conduction band no longer increases with T and the conductivity is mainly limited by phonons, which results in a slight decrease of these parameters. This model should be imperatively tested by conductivity and Hall measurements as functions of temperature and vacancy concentrations. However, a qualitative confirmation is given by the Mott criterion,[18] which gives the conditions for the formation

of an impurity band:

$$a_d(N_d)^{1/3} > 0.26 , \tag{26}$$

where N_d is the donor concentration and a_d the Bohr radius of the donor. In the hydrogenoid model for shallow donors, a_d is related to the thermal ionization energy E_d of the defect by

$$a_d = \frac{1}{\varepsilon_r} a_H \frac{E_H}{E_d} , \tag{27}$$

where $\varepsilon_r = 10.2$ is the dielectric constant of gallium oxide, $a_H = 0.53$ Å, and $E_H = 13.6$ eV are the Bohr radius and the ionization energy of hydrogen atom. By taking $E_d \approx 0.04$ eV for shallow donors in gallium oxide,[8] one obtains $a_d \approx 18$ Å. From expression (26) one gets $N_d > 3\times10^{18}$ cm^{-3} for the critical donor concentration. This value seems to be actually reached since our crystals contain about 10^{19} spins/cm^{-3} at room temperature, so that the hypothesis of an impurity band due to oxygen vacancies is qualitatively confirmed. Another qualitative confirmation is given by the temperature dependence of the line distortion for large samples (see Sec. IV C). The donor concentration of the crystals studied by Lorenz[8] was 2×10^{18} cm^{-3}, which is slightly below the Mott criterion. This could explain the low conductivity at 4 K found by this author, with $(\sigma_{300\text{ K}}/\sigma_{4\text{ K}}) \approx 30$, compared to our crystals which are characterized by $(\sigma_{300\text{ K}}/\sigma_{4\text{ K}}) \approx 1.4$.

B. Hysteresis induced by magnetic-field sweep

The nuclear field B_n induced by the Overhauser effect is bistable at high microwave power, resulting in a resonance field and a line shape which depend on the magnetic-field sweep direction. Figures 9 and 10 show some selected examples of bistable EPR lines at room temperature and at 150 K, recorded for different values of the incident microwave power. Increasing P from 0.2 mW (not represented) to about 2.5 mW results in a small Overhauser shift and a distortion from the Lorentzian shape. For $P > 5$ mW, the distortion is more pronounced and both the Overhauser shift and the line shape become dependent on the direction of variation of B_0 because of the onset of a bistable nuclear field. These effects increase with P. Note that the EPR lines at low temperature and high microwave power (Fig. 10) consist only of negative deviations from the baseline, although they represent first derivatives of the microwave absorption. This implies that the double integral of the EPR lines tends toward infinity. It is thus of fundamental interest to determine if this peculiar line shape is intrinsic to the bistability phenomenon or if it is due to some other undetermined reason. To gain insight into these manifestations of the electron-spin bistability we simulated the EPR lines by using a simple line-shape model.

The main approximation in our calculations is that we assume that the spin system obeys steady-state conditions $d\langle S_z\rangle/dt = 0$ and $d\langle I_z\rangle/dt = 0$ at any moment during the magnetic-field sweep, thus at each point of the resonance line. These conditions impose that the sweeping time through the resonance is much larger than the electron-spin relaxation time T_1 and the nuclear relaxation time T_x. This is a reasonable assumption since the sweeping time corresponding to the spectra of Figs. 9 and 10 is equal to 100 s, while T_1 is lower than 2×10^{-7} s (Fig. 7) and T_x lies between 0.1 and 0.5 s (Ref. 4).

The microwave power P_{abs} absorbed by the sample is proportional to the y component of the electron spin in the rotating frame $\langle S_y'\rangle$, given by the following expression:[9]

$$\langle S_y'\rangle = \frac{\gamma B_1 T_2}{1+\gamma^2 T_2^2 (B_0 - h\nu/g\beta)^2 + \gamma^2 T_1 T_2 B_1^2} \langle S_z^0\rangle . \tag{28}$$

Since we are dealing with the Overhauser effect, B_0 is replaced by $B_{\text{eff}} = B_0 + B_n$ in expression (28). The EPR signal being detected by modulation of the magnetic field B_0, the intensity I_{EPR} of the signal is proportional to

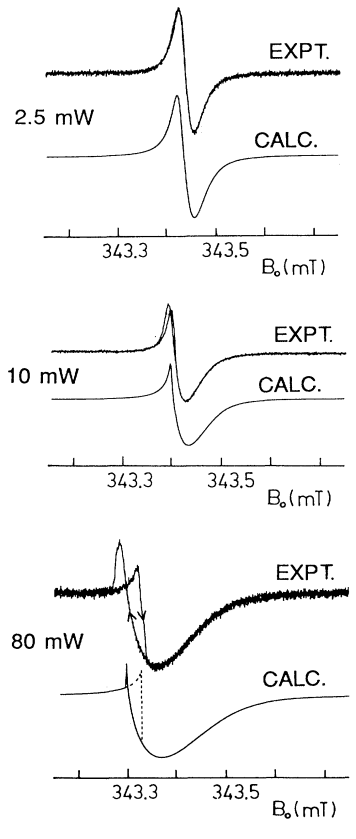

FIG. 9. Selected experimental and calculated EPR spectra at room temperature. Microwave frequency $\nu = 9437$ MHz; sweeping time 100 s; time constant 41 ms; modulation amplitude 0.01 mT. The parameters of the calculated spectra are $T_1 = T_2 = 2.0\times10^{-7}$ s, $(\Delta B_{\text{ov}})_{\max} = 0.213$ mT; $h\nu/g\beta = 343.45$ mT. The microwave field B_1 is related to P by $P = 5.2\times10^4 B_1^2$. The scaling factor I_0 is obtained from a fit of the calculated spectrum to the experimental one at $P = 2.5$ mW. The same value of I_0 is used for the other spectra.

dP_{abs}/dB_0:

$$I_{EPR} = -I_0 \frac{B_1(B_{eff} - h\nu/g\beta)}{[1+\gamma^2 T_2^2 (B_{eff} - h\nu/g\beta)^2 + \gamma^2 T_1 T_2 B_1^2]^2} \times \frac{dB_{eff}}{dB_0} , \quad (29)$$

where I_0 is a constant depending on both the spectrometer and the sample. From the expression of B_{eff}, one obtains:

$$\frac{dB_{eff}}{dB_0} = 1 + \frac{dB_n}{dB_0} . \quad (30)$$

The term dB_n/dB_0 corresponds to the effect on B_n of the magnetic-field modulation. Since the modulation frequency is 100 kHz and the nuclear relaxation time T_x is of the order of 0.4 s, which corresponds to a frequency of 2.5 Hz, it is clear that the nuclear spins cannot follow the modulation cycles, implying $dB_n/dB_0 \ll 1$ in expression (30). Consequently the EPR intensity vs the external magnetic field can be written as

$$I_{EPR} = -I_0 \frac{B_1(B_0 + B_n - h\nu/g\beta)}{[1+\gamma^2 T_2^2 (B_0 + B_n - h\nu/g\beta)^2 + \gamma^2 T_1 T_2 B_1^2]^2} . \quad (31)$$

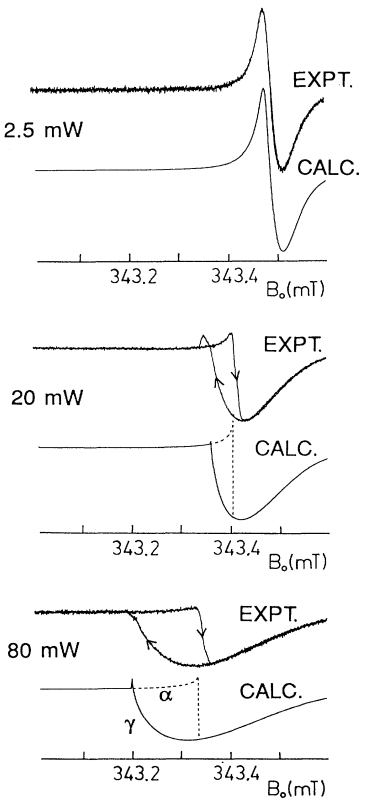

FIG. 10. Selected experimental and calculated EPR spectra at 150 K. Microwave frequency $\nu = 9435.2$ MHz; sweeping time 100 s; time constant 41 ms; modulation amplitude 0.01 mT. The parameters of the calculated spectra are: $T_1 = T_2 = 2.0 \times 10^{-7}$ s; $(\Delta B_{ov})_{max} = 0.47$ mT; $h\nu/g\beta = 343.51$ mT. The scaling factor is obtained by the same procedure as for Fig. 9.

The center of the resonance corresponds to $I_{EPR} = 0$, which is obtained if the condition $B_0 + B_n = h\nu/g\beta$ is satisfied, if B_{eff} is equal to the resonance field of the unsaturated EPR line. Since T_1 and T_2 are known in the entire temperature range 4–300 K (Fig. 7) and since B_1 is determined from $P = KB_1^2$, the calculation of the bistable EPR spectra needs only the determination of B_n and I_0. The nuclear field was obtained by numerical resolution of Eq. (12). For each P value, I_{EPR} was calculated for 400 different values of B_0, leading to a spectral resolution of 1.5 μT. Depending on P and the magnetic field B_0, one obtains one or three values for B_n. In the latter case, two values correspond to stable steady states α and γ, and the third one corresponds to the unstable steady state β. The lowest (highest) value of B_n, corresponding to the α (γ) state, is obtained experimentally upon an upward (downward) sweep of B_0. The intermediate value of B_n corresponds to the unstable state β. In expression (31), I_0 is a scaling parameter which was determined at low microwave power ($P = 2.5$ mW) by a least-squares fit to expression (31) of the experimental unsaturated line. At each temperature, the same value of I_0 was used for all the spectra. Figures 9 and 10 show the comparison between some experimental and theoretical spectra. The agreement may be considered as very satisfying at 150 K if we note that there is no adjustable parameter if we except the scaling factor I_0 determined at low microwave power. The agreement is not so perfect at room temperature, and particularly at high microwave power and for negative variation of the magnetic field (Fig. 9). In that case, the EPR exhibits a positive component which is not reproduced in the simulation. Preliminary simulations show that this discrepancy could originate from the stationary condition $d\langle I_z \rangle/dt = 0$, which is not rigorously satisfied at room temperature. It could also be a consequence of the skin-depth effect (see Sec. IV C).

The principal features of bistable EPR lines can be deduced from the calculated spectra.

(i) The theoretical spectra exhibit a discontinuity, particularly evident for the upward sweep case. This discontinuity is the manifestation of the abrupt change of the nuclear field from the lower branch α to the upper branch γ of the bistable system (see Fig. 2). However, despite the fact that the upward sweep spectrum effectively varies rapidly in a magnetic-field range where a discontinuity is expected, it is clear that the latter is not really observed. This discrepancy originates from the fact that the steady-state condition $d\langle I_z \rangle/dt = 0$ cannot be maintained at a field B_0, where B_n varies abruptly, because of the relatively long nuclear relaxation time T_x, so that expression (31) is not strictly valid at a discontinuity.

(ii) As found experimentally, increasing P results in a decrease of the positive part of the EPR, which becomes close to zero at low temperature and high microwave

power for both sweep directions (Fig. 10, $P=80$ mW). This feature is a direct consequence of the fact that the nuclear spins cannot follow the magnetic-field modulation [$dB_{\rm eff}/dB_0 \approx 1$ in expression (29)]. If this condition is not taken into account in the calculation, both upward and downward spectra contain very narrow and intense positive components at B_0 values corresponding to $\alpha \leftrightarrow \gamma$ switching. In principle, these positive components could appear at very low-frequency modulation.

(iii) We also calculated the theoretical spectrum of the unstable steady-state β. Figure 11 shows an example of simulation corresponding to $T=150$ K and $P=158$ mW. This spectrum (solid line) was calculated with the same procedure as for α and γ states (represented by dotted lines), by allowing in expression (31), the third (unstable) solution of Eq. (12). The β spectrum also exhibits a peculiar line shape, composed of a rounded positive component, at field values where positive parts of the upward and downward spectra are lacking. Only the high-field part of the spectrum is common to the other spectra. Obviously, it is not possible to record experimentally this "unstable" EPR line under steady-state sweep conditions. As shown previously (Fig. 3 in Ref. 4), the β state would be theoretically stable (and the α and γ states unstable) if the time is reversed.

(iv) Figure 12 shows the experimental variations (black circles) of the width of hysteresis of the Overhauser shift, defined as $\Delta B_{\rm ov}^{\downarrow} - \Delta B_{\rm ov}^{\uparrow}$, vs the saturation factor at the center of resonance, $s_r = P/(a+P)$, at room temperature, and at 150 K. $\Delta B_{\rm ov}^{\downarrow}$ was defined previously and $\Delta B_{\rm ov}^{\uparrow}$ is the B_0 value at which the upward EPR line crosses the baseline. The saturation factor s_r corresponds to expression (4) with $B_{\rm eff} = h\nu/g\beta$, and with the constant a given by expression (18). The theoretical variations (solid lines) were obtained from the calculated spectra. The agreement between experimental and theoretical variations is fair at 150 K, and a decrease of the width of hysteresis is

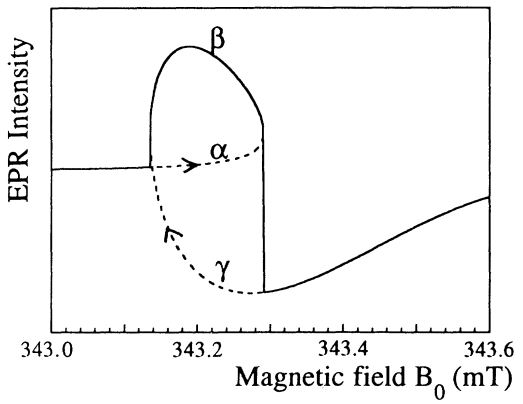

FIG. 11. Typical example of calculated EPR spectra in bistable regime. The dotted lines represent the spectra calculated for the stable steady states α (upward sweep) and γ (downward sweep) of the nuclear field. The solid line represents the spectrum calculated for the unstable steady-state β. Parameters of the calculation: $T=150$ K; $P=158$ mW; $T_1=T_2=2.0\times10^{-7}$ s; $(\Delta B_{\rm ov})_{\rm max}=0.47$ mT and $h\nu/g\beta=343.5$ mT.

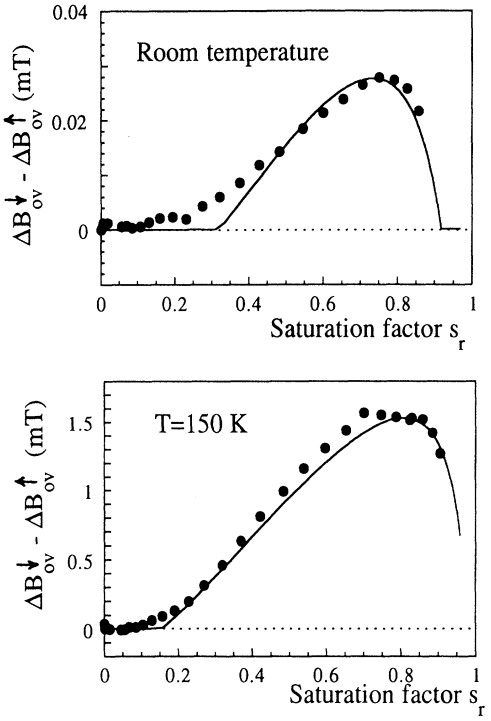

FIG. 12. Variation of $\Delta B_{\rm ov}^{\downarrow} - \Delta B_{\rm ov}^{\uparrow}$ vs the saturation factor at resonance $s_r = P/(a+P)$ at room temperature and at 150 K, with $a = K/\gamma^2 T_1 T_2$ and $K = 5.2\times10^4$ mW/mT^{-2}. $\Delta B_{\rm ov}^{\downarrow}$ and $\Delta B_{\rm ov}^{\uparrow}$ are the Overhauser shifts measured for negative and positive variations of B_0, respectively. Circles: experimental values. Solid line: calculated. The dotted line represents the case of a monostable system.

predicted at a high saturation factor. At room temperature, bistability occurs for $0.3 \le s_r \le 0.9$, with a maximum at $s_r \approx 0.75$. It appears however that bistability at room temperature appears experimentally at a value of s_r lower than the critical value 0.3. This is also evident on the simulated spectrum at $P=10$ mW (Fig. 9) where a monostable resonance is predicted, while the experimental spectrum exhibits a small hysteresis. In our opinion, this small discrepancy is also a consequence of the assumption of a steady-state condition $d\langle I_z \rangle/dt = 0$ in the calculation.

C. Effect of sample size

Up to now, bistability has been studied for very small samples, and we obtained good agreement between experiment and theory only in that case. Several effects result from an increase of the sample volume V. At low microwave power, it first produces an increase of the peak-to-peak linewidth from $\Delta B_{\rm pp}^0 \approx 0.04$ mT at room temperature for a sample volume $V \approx 0.01$ mm^3, to $\Delta B_{\rm pp}^0 \approx 0.1$ mT for $V \approx 1$ mm^3. This effect is due to imperfections of large crystals, which can be considered as a mosaic of small "perfect" crystals. This mosaic effect is responsible of an inhomogeneous broadening of the EPR line. Another sample-size effect is a distortion of the unsa-

turated line due to the high conductivity of the compound. An electromagnetic field is damped and dephased in a conducting sample.[11] The penetration depth δ (the skin depth) in the sample depends on the frequency ω of the field and on the conductivity σ of the material:

$$\delta=\sqrt{2/4\pi\sigma\omega}\ . \tag{32}$$

In the case of β-Ga_2O_3 crystals with conductivity of the order of $10^2\ \Omega^{-1}\,cm^{-1}$ in a 9.4-GHz microwave field, the skin depth is equal to $\delta\approx 5\times10^{-3}$ cm. Consequently, the microwave field penetrates completely only in crystalline platelets with small thickness d compared to the skin depth δ, such as those studied in this work. In large samples, this effect is responsible for a mixing of absorption and dispersion in the EPR line. The mixing coefficient is a function of d/δ. The resulting distortion of the unsaturated line (Dysonian line shape) is quantified by the A/B ratio (inset in Fig. 13). For example, this ratio varies in our case from $A/B=1$ (purely Lorentzian shape) for a sample volume $V\approx0.01$ mm^3, to $A/B=2.5$ for $V\approx2$ mm^3. Figure 13 shows the temperature dependence of the A/B ratio for a sample of thickness larger than the skin depth. The increase of A/B is directly related to the increase of d/δ with T, which is due to the increase of conductivity. A/B varies only from 1.25 to 1.45 between 4 K and room temperature, which agrees with the small difference between 4 K and room temperature conductivity of our samples. In particular, the constant value of A/B between 4 and 50 K is consistent with an electronic motion in an impurity band, with a conductivity limited by impurity or defect scattering. The increase of A/B at higher temperature and its stabilization above about 200 K reflects the thermal excitation of electrons in the conduction band and the conductivity limited by phonon scattering at high temperature, as proposed in Sec. IV A.

The most striking sample-size effect is the strong modification of the line shape and the loss of bistability at high microwave power (Fig. 14). Increasing the sample

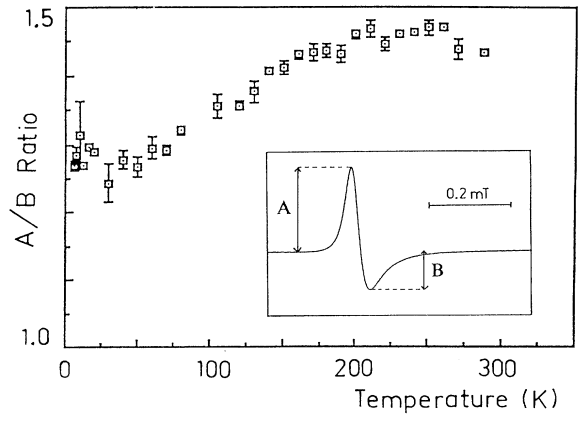

FIG. 13. Temperature dependence of the ratio A/B of the EPR line for a β-Ga_2O_3 crystal of size $0.23\times2.17\times1.3$ mm^3. Microwave power $P=0.2$ mW. The fields B_0 and B_1 are parallel to the crystallographic axes a and b, respectively. Inset: example of Dysonian EPR line at room temperature.

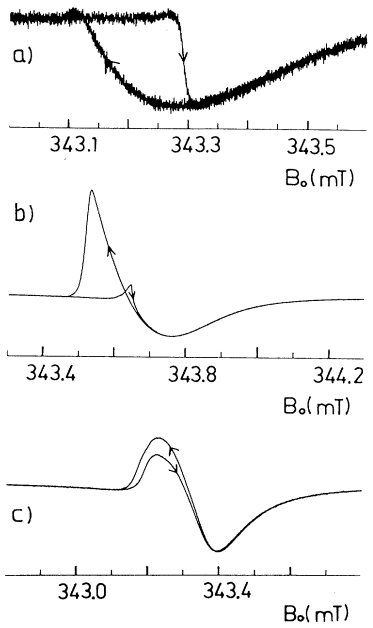

FIG. 14. Effect of sample size on the line shape under bistability conditions at $P=158$ mW and at 150 K. (a) Sample size $0.08\times1.8\times0.27$ mm^3. (b) Sample size $0.23\times2.17\times1.3$ mm^3. (c) Sample size $1.0\times2.34\times1.43$ mm^3. The other parameters are the sweeping time 100 s, the time constant 0.41 ms, and the modulation amplitude 0.01 mT.

size results in an increase of the positive part of the EPR line, especially for the downward sweep case, and a reduction of the width of hysteresis. This effect could explain the excess in the positive part observed for the downward sweep lines at room temperature, compared to the calculated ones (Fig. 9). Figure 14(c) shows that the hysteresis almost disappears for large samples. These two features are also due to the skin effect. The growth of the positive part of the signal is due to the dispersion component of the EPR signal, which increases with the sample size. The gradient of B_1 in the sample results in a distribution of Overhauser shifts for both upward and downward spectra, which in turn results in a decrease of the apparent width of hysteresis.

Our previously reported bistable electron-spin resonance spectra[4] exhibit shapes which are slightly different from those reported in this paper. The reason is that the former spectra correspond to samples larger than the skin depth of the compound, with a large positive part for the downward sweep lines. The observed hysteresis was also reduced, so that the Overhauser shift ΔB_{ov} at room temperature did not depend on field sweep direction. However, it is clearly shown in this work that if the skin effect is suppressed, a significant hysteresis of the Overhauser shift is observed for small samples at room temperature (Fig. 9).

D. Hysteresis induced by variation of the incident microwave power

We showed in Sec. II that, if the conditions for bistability are satisfied, the EPR intensity should also exhibit

hysteresis with the microwave power as control parameter. We have verified this prediction with the same samples as those used for the magnetic-field-induced bistability. B_0 was set at a constant value in the magnetic-field range where bistability occurs, and the EPR intensity was measured at microwave power values in the range 0.2 mW ($B_1=2\times10^{-3}$ mT) to 200 mW ($B_1=6.2\times10^{-2}$ mT). Figure 15 shows the experimental microwave power dependence of the EPR intensity for upward (open circles) and downward (solid circles) variations of P at room temperature and at 150 K. One clearly observes a hysteresis which is particularly important at low temperature. At 150 K, and for P values between 50 and 100 mW, the EPR intensity is very small for positive variations of P, while it becomes large and of opposite sign for the negative variation. Figure 15 also shows the theoretical variations $I_{\rm EPR}=f(P)$ calculated by the same procedure as in Secs. II and IV B. These curves are in qualitative agreement with the experimental variations. In particular, the width of hysteresis is accurately predicted.

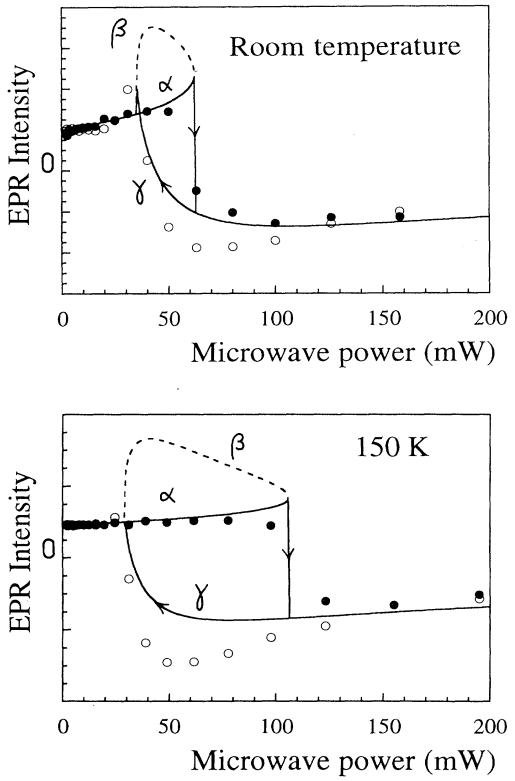

FIG. 15. Microwave power dependence of the EPR intensity in bistable regime, at room temperature (top) and at 150 K (bottom). Solid circles and open circles correspond to positive and negative variations of P, respectively. Solid lines correspond to theoretical variations, calculated for the steady states α and γ. Dotted lines correspond to the variation calculated in the case of the unstable state β. Parameters at room temperature: $B_0=343.34$ mT; $T_1=T_2=2.0\times10^{-7}$ s $(\Delta B_{\rm ov})_{\rm max}=0.23$ mT; $h\nu/g\beta=343.45$ mT. Parameters at 150 K: $B_0=343.32$ mT; $T_1=T_2=2.0\times10^{-7}$ s; $(\Delta B_{\rm ov})_{\rm max}=0.47$ mT; $h\nu/g\beta=343.51$ mT.

It is noteworthy that the theoretical variations $I_{\rm EPR}=f(P)$ have precisely the same shape as the EPR spectra themselves $[I_{\rm EPR}=f(B_0)]$, as shown by comparison of Figs. 15 and 11. This similitude is also true for the theoretical variations $I_{\rm EPR}=f(P)$ in the case of the unstable steady state β (dotted lines in Fig. 15), which is very similar to the theoretical EPR spectrum of the β state (Fig. 11).

V. SUMMARY AND CONCLUSION

We have studied in this paper the bistable Overhauser shift of conduction electrons in semiconducting gallium oxide β-Ga_2O_3. This phenomenon originates from the existence of two stable steady states of the nuclear field B_n, created by dynamic nuclear polarization (Overhauser effect). The principal results are the following.

(i) The temperature dependence of NAf indicates that from 4 to 300 K, the electronic wave function is essentially made of 4s gallium orbitals. It is proposed that the oxygen vacancies, in the form of $V_{\rm O}^{\times}$ (or F) centers and $V_{\rm O}^{\bullet}$ (or F^+) centers, form a partially occupied shallow impurity band responsible for the low-temperature conductivity.

(ii) The magnetic bistability of electron spins is interpreted within the framework of intrinsic bistability of noninteracting conduction electrons. Each electron submitted to an external magnetic field B_0 and to a microwave field B_1 of frequency ν, experiences an effective field $B_{\rm eff}$ which actually depends on the direction of variation of one of the three control parameters B_0, B_1, or ν.

(iii) The hysteresis of the experimental EPR spectrum manifests itself by Overhauser shifts and line shapes which depend on the magnetic-field sweep direction. The spectra can be accurately simulated if we assume steady-state spin polarizations $(d\langle S_z\rangle/dt=0$ and $d\langle I_z\rangle/dt=0)$ during magnetic-field sweep. The experimental microwave power dependence of the hysteresis of the Overhauser shift $\Delta B_{\rm ov}^{\downarrow}-\Delta B_{\rm ov}^{\uparrow}$ is also in good agreement with theory.

(iv) For fixed values of B_0 and ν, the variation of the EPR intensity with the microwave power P exhibits a significant hysteresis, in agreement with theoretical predictions. In particular, the shapes of the $I_{\rm EPR}=f(P)$ curves are closely similar to the EPR line shapes $I_{\rm EPR}=f(B_0)$.

(v) The magnetic bistability of conduction electrons is sensitive to the crystal size. An accurate simulation of the EPR spectra is possible only if the sample thickness is smaller than the skin depth of the compound. The consequence of this effect is that bistability disappears with large samples.

Finally, it is noteworthy that β-Ga_2O_3 is an inorganic conducting material which exhibits an Overhauser shift at high temperature. Up to now, only organic conductors were known to exhibit this effect at room temperature.[13,19] We have previously shown[4,7] that bistability is expected if the EPR line is sufficiently narrow and if the product $I(I+1)NAf$ is sufficiently high. The first condition is in favor of organic conductors since a compound such as difluoranthenyl-phosphorhexafluoride (FA_2PF_6)

exhibits a linewidth as small as 10^{-3} mT or less, while it is about 5×10^{-2} mT or less for β-Ga_2O_3. However the product $I(I+1)NAf$ is larger than 11×10^3 MHz at room temperature in this compound, while it is only about 40 MHz for FA_2PF_6. The linewidth of gallium oxide, which is very narrow for an inorganic conductor, and the high value of $I(I+1)NAf$ are directly at the origin of the bistability of the Overhauser effect in this compound.[7] The reasons why such values are reached for gallium oxide, and in particular its small linewidth, are not yet clearly understood. They probably reflect particular transport properties of this compound, and further work is needed to understand the relation between the magnetic bistability of conduction electrons of β-Ga_2O_3 and its crystallographic and electronic structures.

ACKNOWLEDGMENTS

The authors thank Rhone-Poulenc for financial support. We are indebted to A.M. Lejus for her contribution in the crystal growth of β-Ga_2O_3 and to D. Simons for technical assistance. Laboratoire de Chimie Apliquée de l'Etat Solide is Unité Associée au Centre National de la Recherche Scientifique No. 1466.

*Author to whom correspondence should be addressed.

[1]A. E. Kaplan and A. Elci, Phys. Rev. B **29**, 820 (1984).
[2]J. I. Kaplan, Phys. Rev. **99**, 1322 (1955).
[3]M. Gueron and C. Ryter, Phys. Rev. Lett. **3**, 338 (1959); C. Ryter, *ibid.* **5**, 10 (1960).
[4]E. Aubay and D. Gourier, J. Phys. Chem. **96**, 5513 (1992).
[5]A. Overhauser, Phys. Rev. **92**, 411 (1953).
[6]I. Solomon, Phys. Rev. **99**, 559 (1959).
[7]E. Aubay and D. Gourier, Solid State Commun. **85**, 821 (1993).
[8]M. R. J. Lorenz, J. Phys. Chem. Solids. **28**, 403 (1967).
[9]A. Abragam and B. Bleaney, *Resonance Paramagnétique Électronique des Ions de Transition* (Presse Université de France, Paris, 1971), p. 119.
[10]F. Bozon-Verduraz, C. Potvin, and G. Pannetier, J. Chim. Phys. (France) **67**, 1608 (1970).
[11]F. J. Dyson, Phys. Rev. **98**, 349 (1955); G. Feher and A. F. Kip, *ibid.* **98**, 337 (1955).
[12]C. P. Poole, *Electron Spin Resonance* (Wiley, New York, 1983), p. 597
[13]W. Stöcklein and G. Denninger, Mol. Cryst. Liq. Cryst. **136**, 335 (1986).
[14]S. Geller, J. Chem. Phys. **33**, 676 (1960).
[15]T. Albright, J. K. Burdett, and M. H. Wangbo, *Orbital Interaction in Chemistry* (Wiley, New York, 1985), p. 229.
[16]A. Raüber and J. Schneider, Phys. Status Solidi **18**, 125 (1966).
[17]V. I. Vasil'tsiv, Ukr. Fiz. Zh. **33**, 1320 (1988).
[18]N. F. Mott and W. D. Twose, Adv. Phys. **10**, 107 (1961); P. P. Edwards and M. J. Sienko, J. Am. Chem. Soc. **103**, 2967 (1981).
[19]G. Denninger, W. Stöcklein, E. Dormann, and M. Schwoerer, Chem. Phys. Lett. **107**, 222 (1984).